PTAC - AUPRF Pileated Woodpecker Report

Prepared by: Brendan Casey, Harsimran Bains, Erin Bayne

Cover photo by: Kyle Taylor

December 2025

Table of Contents

Executive Summary

The Pileated Woodpecker (hereafter PIWO) is a keystone species whose nest cavities provide essential breeding habitat for dozens of migratory birds and mammals. Under the Migratory Bird Convention Act (MBCA) and the Migratory Birds Regulations, 2022 (MBR 2022), PIWO nest cavities are protected from damage or destruction — and provincially under Alberta's *Wildlife Act* and *Public Lands Act* (Province of Alberta 2000a, 2000b) — creating a clear need for reliable tools that help industry locate, manage, and avoid cavity-bearing trees during project planning and implementation. If a cavity is encountered during a project, a buffer zone of a minimum width of 100m of undisturbed vegetation must be established (MSSC, 2023). To meet this need, we developed an integrated framework to detect, map, and monitor PIWO nest cavities, and support regulatory compliance.

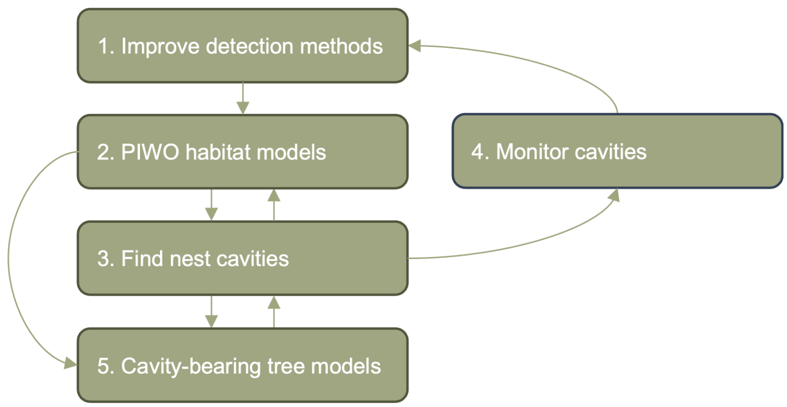

Across 2023–2025, our team advanced each component of this framework (see Table 1). Key achievements include optimizing PIWO drumming detection methods, developing Alberta-wide PIWO habitat maps, conducting large-scale cavity-bearing tree surveys, and implementing an ongoing nest cavity monitoring program.

Research on PIWO drumming behaviour identified an optimal detection window in early April near sunrise, reducing effort to confidently assess site use from 32 to 10 one-minute recordings. These improved detection estimates strengthened the habitat modelling process by providing higher-quality presence data. Using these refined detections, we mapped PIWO habitat across Alberta by integrating land cover, climate, Landsat, and Sentinel-2 data, producing a 100-m provincial habitat suitability map that was subsequently validated with cavity-bearing tree locations.

Using this predictive map, field crews conducted 1,180 ha of cavity searches across the province. To support this work, we developed and implemented a standardized 1-ha cavity search protocol, which is now widely adopted by multiple municipalities, environmental consultants, and the Government of Alberta. We found an average of 0.5 cavities/ha, with a strong skew towards smaller sized cavities. PIWO sized cavities (> 7.6 cm) were more difficult to find, with densities of 0.040-0.007 cavities/ha, suggesting that large cavities are found less frequently on the landscape However, cavities were found across the full range of predicted habitat suitability,, indicating that restricting searches to only the highest-suitability areas identified by the acoustic model would miss many cavities.

To improve on the acoustic-based PIWO habitat models and identify where cavities are most likely to occur within stands, we used the cavity-bearing tree locations documented through our standardized search protocols to develop light detection and ranging (LiDAR) based cavity-bearing tree models. Despite the tree crown level measurements provided by LiDAR, these models did not improve predictive performance. Nevertheless, the resulting crown maps remain valuable, helping field crews target large or stressed aspen more likely to contain cavities.

We developed and implemented a long-term cavity monitoring program to track cavity longevity, reuse, and broader cavity-community dynamics. In 2025, we revisited 40 previously documented cavities and confirmed 10 cases of reuse, providing early insight into how long PIWO and other cavity users continue to occupy old sites. To complement this monitoring, we developed a framework for using autonomous recording units (ARUs) to locate drumming and vocalizing PIWO. Using ARUs deployed at known nests, feeding sites, and random control locations, we quantified behavioural differences among site types and found that drumming and acoustic behaviour can be used to distinguish nearby nest cavities from feeding snags. Building on this, we deployed more than 100 ARUs at varying distances from recently active cavities to develop distance-to-cavity models, a key step toward tools that could reduce ground search effort by allowing cavities to be identified directly from ARU recordings.

Additional tool development included a province-wide camera-deployment experiment evaluating whether ground-based cameras can reliably detect which species using PIWO cavities from ground based photographs, and the creation of a Google Earth Engine web application that provides partners with access to predictive maps, cavity locations, and model outputs.

Together, the tools, methods, and maps developed in this project form a comprehensive detection-to-monitoring pipeline for PIWO nest cavities.

Table 1: Progress overview.

Activity	Progress
Optimized Sampling Methods	Completed research quantifying how survey timing, temperature, and day length influence PIWO detectability. Identified the optimal detection window (early April, near sunrise), reducing effort required for 90% certainty of site use from 32 to 10 one-minute recordings.
Refined Modelling Methods	Evaluated how modelling choices—response variable, land-cover dataset, and spatial scale—influence predictive accuracy. Built regional habitat models (65–70% accuracy) showing biomass and canopy closure as consistent predictors.
Improved Acoustic Occupancy Model and Map	Mapped PIWO habitat by integrating land cover, climate, Landsat, and Sentinel-2 data. Produced a 100-m provincial habitat suitability map which was validated using cavity-bearing tree locations.
LiDAR-Based Sub-Models	Built high-resolution LiDAR sub-models to refine predictions. LiDAR variables were consistently dropped during model simplification, providing no added predictive value over the Alberta-wide model. Demonstrated that broad-scale spectral/land-cover predictors already capture key PIWO habitat features (older aspen, mixedwoods).
Cavity-Bearing Tree Model (Single-Tree LiDAR Analysis)	Mapped individual crowns, calculated crown-level LiDAR and spectral metrics, and built cavity-suitability models. Models showed no improvement over provincial habitat models—LiDAR metrics did not add predictive power. However, crown maps remain valuable for targeting large/decayed trees during fieldwork. Will revisit models as more cavity data accumulate.
Used Predictive Map to Inform Fieldwork	Classified habitat predictions into four suitability bins and implemented stratified random sampling across Alberta. Built a 1-ha sampling framework using 100 × 100 m plots to select search locations.
Developed Standardized Cavity Search Protocols	Developed a standardized 1-ha transect search protocol now used by the cities of Edmonton and Red Deer, the Government of Alberta, and multiple environmental consultants. Created a public cavity-tracking app through Epicollect.

Fieldwork	Conducted almost 1200 ha of systematic searches/ Deployed 188 ARUs for validation of acoustic model. Documented 1,450 cavities (overall density = 1.164 cavities/ha). Identified viable cavities using wireless pole cameras and addressed limitations (equipment, access, height constraints).
Monitoring Cavities (Ongoing Program)	Revisited 40 cavities in 2025; confirmed 10 reused. Continued collaboration with Royal Alberta Museum. Tracking cavity longevity, reuse patterns, and secondary cavity users.
Evaluating Drumming Behavior (ARU-Based Analyses)	Developed an ARU-based detection framework; established optimal seasonal/daily timing. Deployed ARUs at nests, feeding sites, and random locations. Demonstrated significant differences in acoustic signatures among site types ($\chi^2 = 2067$, $p < 2.2e-16$). Multinomial models showed best predictors of cavity type include drums, adult calls, juvenile calls, and distance. Deployed 100+ ARUs in 2025 for distance–to–cavity model development.
Camera Deployment Experiment	Began systematic evaluation of Reconyx Hyperfire cameras to assess bird detectability at varying distances and heights. Installed experimental feeder-camera arrays across Alberta. Data currently being processed in WildTrax. Expected to improve safe, ground-based cavity-monitoring methods.
Google Earth Engine Web Application	Developed a GEE web app to share predictive maps, field search locations, cavity detections, and model outputs. Will serve as the foundation for future fieldwork and model updates.

1. Background

The *Migratory Birds Convention Act, 1994* (MBCA) is legislation designed to protect migratory birds, their nests, and eggs across Canada. The MBCA is implemented by specific regulations, one of which is the Migratory Birds Regulations (MBR). These regulations were created to address overharvesting and unregulated trade of migratory birds. In 2022, Environment and Climate Change Canada introduced a modernized version of the MBR. Some of the key changes made were to the regulations for nest protections. Under the MBR 2022, it is prohibited to damage, destroy, disturb, or remove nests of all migratory birds when they contain a live bird or viable egg. Additionally, 18 species (identified on Schedule 1) receive year-round nest protection, regardless of whether the nest contains live birds or eggs, until those nests are considered abandoned. This includes migratory birds who reuse their own nest from one year to the next, as well as resident birds whose nest cavities are reused by migratory birds. Under this regulation, a nest is considered abandoned if it remains unused by migratory birds during the designated wait time for that species.

Cavities in trees are used as breeding sites and refuges by many species in forest ecosystems (Martin and Eadie 1999, Martin et al. 2004). These cavity nesters can be classified into 3 guilds based on the way they acquire cavities. Primary excavators, such as woodpeckers, create cavities for nesting and roosting. Weak cavity excavators may excavate their cavities, use naturally occurring holes, or may use cavities created by primary excavators. The third guild, secondary cavity nesters, includes a variety of migratory birds and small mammals that require cavities but cannot excavate them. There is some evidence in certain regions that cavity-nesting species, birds in particular, are limited by the availability of cavities more than food or territorial space (Ke *et al.* 2023).

The PIWO is a resident bird found year-round in deciduous, coniferous, or mixed forests (Bull and Jackson 2020). PIWOs typically excavate cavities in dead or unhealthy live trees with large diameters (Drapeau *et al.* 2009, Bull and Jackson 2020). Cavities excavated by PIWOs are some of the largest and may serve as nesting or roosting sites for at least 38 other species of birds (Hoyt 1957; Bonar 2000, 2001). As a result, PIWOs are considered a keystone species. Additionally, woodpeckers can serve as reliable indicators of bird richness and forest health (Drever et al. 2008).

Under the amended MBCA, PIWO cavities are provided with Schedule 1 protection (Government of Canada 2023). A cavity is protected for 36 months from the date it is declared on Environment and Climate Change Canada's (ECCC) reporting portal (not from the date it is found in the field) and can only be disturbed, damaged, removed, or destroyed once that period has elapsed without use by other migratory bird species. Active PIWO nest cavities are also protected provincially in Alberta under the *Wildlife Act* and the *Public Lands Act* (Province of Alberta 2000a, 2000b).

The primary objective of our project is to improve our ability to locate and manage activities around PIWO nests, ensuring compliance with regulatory protections.

2. Optimizing Pileated Woodpecker sampling and modelling methods

Austin Zeller, a 2024 MSc graduate, focused his research on improving habitat models for PIWO by optimizing sampling and modelling methods. His thesis addressed several key gaps in provincial monitoring and modelling efforts by: (1) examining how temporal variation in PIWO drumming affects detectability, (2) identifying the environmental conditions that influence drumming behaviour, (3) improving habitat model performance by using data collected during peak detectability periods, and (4) evaluating how modelling decisions—such as the choice of response variable, land-cover dataset, and spatial scale—affect predictive accuracy.

2.1 Detectability

Austin's research demonstrated that survey timing has a substantial influence on the ability to detect PIWO using acoustic recordings. He found that drumming activity peaks near sunrise in early April, before the period that many bird monitoring programs operate. Drumming frequency was strongly shaped by day length and mean daily temperature, with peak detection occurring when mean temperatures were around 0°C. These results show that both static seasonal factors and short-term environmental conditions drive variability in detectability. Importantly, his work showed that conducting surveys within the optimal seasonal and daily windows can dramatically increase survey efficiency—reducing the required effort to achieve 90% confidence in site use from 32 one-minute surveys under typical June conditions to 10 one-minute surveys when timed during the April peak.

2.2 Habitat Models

Using data collected during optimal detection periods, Austin built regional PIWO habitat models to identify which environmental variables best predict habitat use across Alberta's boreal forest. Our first model had only moderate predictive accuracy (area under the curve (of the ROC) (AUC) = 65–70%), the models consistently highlighted two key predictors: biomass, which was positively associated with PIWO use, and canopy closure, which showed a negative association. These findings reinforce the species' reliance on mature and old forests characterized by gap dynamics and large-diameter trees. Austin also demonstrated that the source and scale of land-cover data play critical roles in model performance. Among the datasets evaluated, only the Beaudoin *et al.* (2017) product produced reliable predictors, and broader spatial summaries (565–1000 m buffers) outperformed fine-scale (150 m) measures—indicating that PIWO respond to habitat conditions at relatively large scales which is consistent with their large home ranges relative to many other bird species which in part explains the better accuracy of Austin's models relative to those displayed on the Alberta Biodiversity Monitoring Institute's Biodiversity Browser models.

Austin successfully defended his thesis in January 2024. His thesis chapter, "Temporal Variation in Pileated Woodpecker Behavior: Ecological Explanations and Management Implications," was published in the Journal of Avian Conservation and Ecology (Zeller *et al.* 2024).

3. PIWO Acoustic Occupancy Model

Remote sensing provides an opportunity to substantially improve PIWO habitat models by capturing tree- and stand-level conditions linked to cavity selection. PIWO often excavate cavities in live but physiologically stressed trees affected by wood-decaying fungi or insects (e.g., carpenter ants, bark beetles), a stage sometimes referred to as "green attack," where foliage remains intact despite internal decline (Niemann and Visintini 2004). This stress alters foliar pigments, water content, and crown structure in ways detectable by spectral satellite imagery. Vegetation indices sensitive to moisture and pigment changes—such as NDRS, NDWI, RDI, and red-edge indices from Sentinel-2—have demonstrated strong ability to detect tree stress and early signs of tree decay (Abdullah *et al.* 2019). Combining spectral indices with LiDAR-derived structural metrics captures both canopy condition and forest structure, leading to more predictive PIWO models (Zielewska-Büttner *et al.* 2018, Abdullah *et al.* 2019, Huo *et al.* 2021, Hu and Tong 2022).

Given these advantages, our objectives were to (1) Use spectral indicators of tree senescence and LiDAR derived forest and single-tree structural characteristics to improve habitat models for PIWO and inform ground-based searches of nesting cavities, and (2) Compare PIWO distribution models built with remote sensing data with those based on classified habitat data.

3.1 Methods

Austin Zeller modelled PIWO occupancy for the province of Alberta using landcover predictor variables from Beaudoin *et al.* (Beaudoin *et al.* 2017) and the National Forest Inventory Systems (Gillis *et al.* 2005). We built on his work by developing PIWO occupancy models that incorporated additional variables associated with tree senescence, vegetation structure, and land cover in boosted regression trees (BRTs) to predict the occupancy probability of PIWO . Our newest methodological workflow is illustrated in Figure 2. Analyses were done using R statistical software (R Core Team 2020). Model covariates were gathered, calculated, and extracted using Google Earth Engine (Gorelick *et al.* 2017).

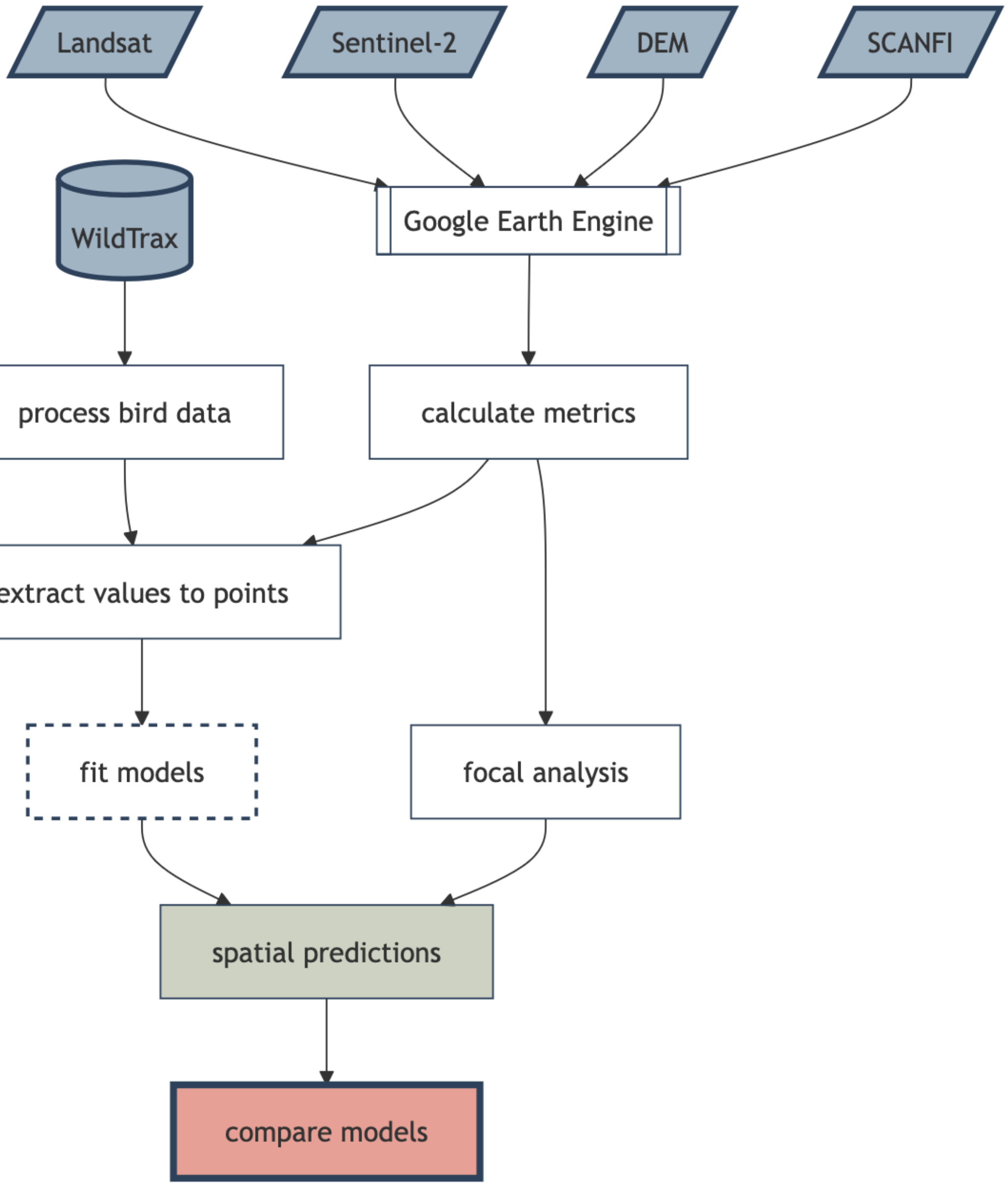

Figure 1: Graphical overview of our methodological workflow.

3.1.1 Study area

We used human and automated and acoustic point counts done across Alberta, Canada, including in the Boreal, Foothills, Parkland, and Rocky Mountain Regions (Natural Regions Committee 2006) (Figure 2).

The Boreal Forest Natural Region spans most of northern Alberta. It is composed of coniferous forests dominated by black spruce (*Picea mariana*), white spruce (*Picea glauca*), and jack pine (*Pinus banksiana*), along with mixedwood forests featuring trembling aspen (*Populus tremuloides*) and balsam poplar (*Populus balsamifera*), and shrubby black spruce fens (Natural Regions Committee 2006). In the

Rocky Mountain region, in western Alberta along the continental divide, vegetation composition changes along an elevation gradient. Higher elevations consist mainly of alpine shrub and meadow, while lower elevations host coniferous and mixedwood forests. Common tree species include lodgepole pine (*Pinus contorta*), Engelmann spruce (*Picea engelmannii*), subalpine fir (*Abies lasiocarpa*), and trembling aspen. The Foothills Natural Region, at the eastern edge of the Rocky Mountains, serves as a transition between the Rocky Mountain and Boreal Regions. At lower elevations, the Foothills is dominated by mixedwood forests of lodgepole pine, white spruce, trembling aspen, and balsam poplar. Lodgepole pine forests are common at higher elevations (Natural Regions Committee 2006). South of the Boreal Forest Natural Region, the Parkland Natural Region consists of cultivated croplands, deciduous forests dominated by trembling aspen and balsam poplar, and grasslands (Natural Regions Committee 2006).

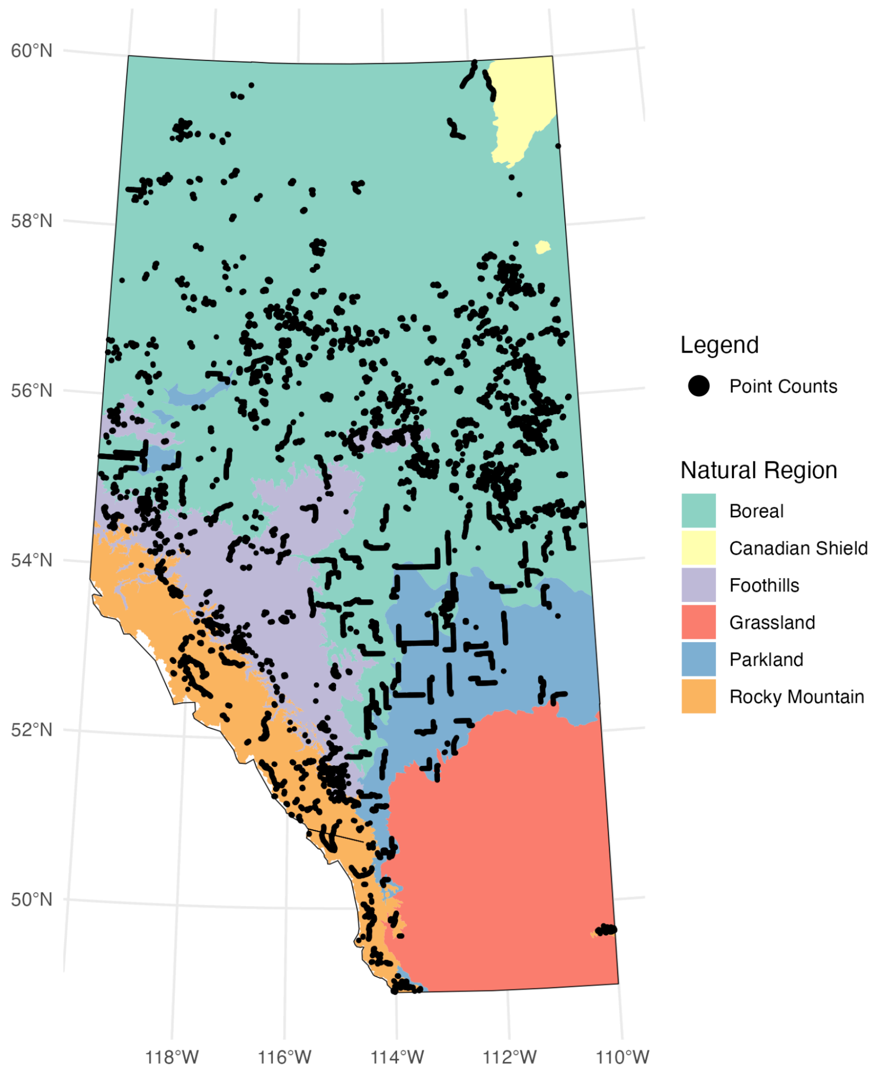

Figure 2: Locations of the point counts used in this analysis overlaid with the Natural Regions of Alberta.

3.1.2 Response variables

We used point count data gathered by the Boreal Avian Modelling Project (BAM) (Boreal Avian Modelling Project 2018) and the University of Alberta's Bioacoustic Unit (http://bioacoustic.abmi.ca/). The data was accessed through www.wildtrax.ca using the *wildRtrax* package in R (MacPhail *et al.* 2024). Our study included point count data from 2010 to 2022, totalling 72,983 point counts across 21,271 locations. Point counts were conducted between 2 AM and 12 PM during the summer (June-September). Wildlife technicians identified PIWO by listening for their calls and drumming patterns. Observers recorded PIWO detections during 1-15 minute point count durations. To account for variations in detection probability from differing sampling efforts, we used the log of sampling effort (the number of survey days multiplied by point count durations) as an offset term in BRTs. Austin Zeller's improved method of detecting PIWO was key to creating the more accurate model described here.

3.1.3 Predictor variables

Predictor variables included a time series of land cover metrics from SCANFI (Guindon *et al.* 2024), vegetation canopy metrics from a model trained with Global Ecosystem Dynamics Investigation (GEDI) LiDAR and Sentinel-2 images (Lang *et al.* 2022), and a Topographic Wetness Index (TWI) calculated from a digital elevation model and water flow direction map (Yamazaki *et al.* 2019)) (Table 2). We derived bioclimatic variables from ClimateNA, a tool that locally downscales historical and future climate data across North America (Wang *et al.* 2016). We summarized 1000 m 30-year climate normals (1991–2020) to each survey point (Table 3.) We also included various spectral measures of vegetation productivity and health from a time series of Sentinel-2 and Landsat 4-9 images. Spectral indices including the Enhanced Vegetation Index (EVI), Green Normalized Difference Vegetation Index (GNDVI), Normalized Burn Ratio (NBR), Normalized Difference Vegetation Index (NDVI), and Leaf Area Index (LAI) were used to capture vegetation productivity. Indices such as the Red Edge Chlorophyll Index (CRE), Distance Red & SWIR (DRS), Disease Stress Water Index (DSWI), Red-edge indices (NDRE1, NDRE2, NDRE3), and the Normalized Difference Water Index (NDWI) were used to measure differences in vegetation health and canopy stress (Table 4). All spectral indices were calculated via the Google Earth Engine JavaScript API.

Table 2: Land cover, vegetation structure, and topographic predictor variables.

Name	Description	Source
Age	Landsat-derived forest age for 2019	Maltman *et al.* (2023)
Biomass	Aboveground tree biomass (tons/ha)	Guindon *et al.* (2024)
Canopy Height	Model trained with GEDI LiDAR to retrieve canopy height from Sentinel-2 images	Lang *et al.* (2022)
Canopy Standard Deviation	Model trained with GEDI LiDAR to retrieve standard deviation of canopy height from Sentinel-2 images	Lang *et al.* (2022)
Crown Closure	Tree canopy coverage (%)	Guindon *et al.* (2024)
Fractional Broadleaf	Proportion of the canopy covered by broadleaf tree species (%)	Guindon *et al.* (2024)
Height	Vegetation height (m)	Guindon *et al.* (2024)
Land Cover Class	Classes include broadleaf forest, mixedwood, conifer forests, shrub, and water	Guindon *et al.* (2024)
Natural Region	Natural regions of Alberta	Natural Regions Committee (2006)
Natural Subregion	Natural subregions of Alberta	Natural Regions Committee (2006)
TWI	Topographic Wetness Index: $\ln(\alpha/\tan\beta)$ where α=cumulative upslope drainage area and β is slope (Sørensen and Seibert 2007)	Yamazaki *et al.* (2019)

Table 3. ClimateNA bioclimatic variables used in the analysis.

Abbr.	Description
AHM	Annual heat moisture index: (MAT + 10) / (MAP / 1000)
bFFP	Julian date on which the frost-free period begins
CMD	Hargreave's climatic moisture index
CMI	Hogg's climate moisture index (mm)
DD_0	Degree-days below 0°C
DD_18	Degree-days below 18°C
DD1040	Degree-days above 10°C and below 40°C
DD5	Degree-days above 5°C
eFFP	Julian date on which the frost-free period ends
EMT	Extreme minimum temperature over 30 years
Eref	Hargreave's reference evaporation
EXT	Extreme maximum temperature over 30 years
FFP	Frost-free period (days)
MAP	Mean annual precipitation (mm)
MAT	Mean annual temperature (°C)
MCMT	Mean temperature of the coldest month (°C)

MSP	Mean summer (May–Sep) precipitation (mm)
MWMT	Mean temperature of the warmest month (°C)
NFFD	Number of frost-free days
PAS	Precipitation as snow (mm)
PPT_at	Autumn (Sep–Nov) precipitation (mm)
PPT_sm	Summer (Jun–Aug) precipitation (mm)
PPT_sp	Spring (Mar–May) precipitation (mm)
PPT_wt	Winter (Dec–Feb) precipitation (mm)
RH	Mean annual relative humidity (%)
SHM	Summer heat moisture index: MWMT / (MSP / 1000)
Tave_at	Autumn (Sep–Nov) mean temperature (°C)
Tave_sm	Summer (Jun–Aug) mean temperature (°C)
Tave_sp	Spring (Mar–May) mean temperature (°C)
Tave_wt	Winter (Dec–Feb) mean temperature (°C)
TD	Temperature difference between MCMT and MWMT (continentality; °C)

3.1.3.1 Spectral indices from Landsat and Sentinel-2

We compiled a time series (2010-2023) of Landsat images from the Landsat 5 Thematic Mapper (bands 4 and 7), the Landsat 7 Enhanced Thematic Mapper, the Landsat 8 Operational Land Imager, and the Landsat 9 Operational Land Imager (Survey 2018, Survey 2019, 2022). We harmonized Landsat 5, 7, 8, and 9 spectral bands using OLS coefficients developed by Roy *et al.* (2016). Images were masked to exclude snow, cloud, and cloud shadow pixels using the QA band generated from the CFMask algorithm

(Foga *et al.*, 2017). We then generated 30 m summer (June-September) median composite images for the following indices: DRS, DSWI, EVI, GNDVI, LAI, NBR, NDVI, and NDWI across the time series.

A similar process was followed to calculate spectral indices from Sentinel-2. A time series (2019-2023) of Sentinel-2 images and masked cloud and snow pixels using the QA60 and MSK_CLASSI_SNOW_ICE bands was created. We generated 10 m summer median composite images for the following spectral indices: CRE, DRS, DSWI, EVI, GNDVI, LAI, NBR, NDRE1, NDRE2, NDRE3, NDRS, NDVI, NDWI, and RDI.

Table 4: Spectral vegetation indices calculated from Landsat and Sentinel-2 time series.

Abbr.	**Name**	**Formula**	**Landsat**	**Sentinel-2**	**reference**
CRE	Red Edge Chlorophyll Index	(RedEdge3 / RedEdge1) - 1		x	Gitelson *et al.* (2003)
DRS	Distance Red & SWIR	sqrt (((RED) * (RED)) + ((SWIR) * (SWIR)))	x	x	Huo *et al.* (2021); Earth Resources Observation And Science (EROS) Center (2017)
DSWI	Disease Stress Water Index	(NIR + Green) / (Red + SWIR)	x	x	Earth Resources Observation And Science (EROS) Center (2017)
EVI	Enhanced Vegetation Index	2.5 * ((NIR - RED) / (NIR + 6 * RED - 7.5 * BLUE + 1))	x	x	Huete (1997)
GNDVI	Green Normalized Difference Vegetation Index	(NIR - Green)/(NIR + Green)	x	x	Gitelson *et al.* (1996)
LAI	Leaf Area Index	3.618 * EVI - 0.118	x	x	Earth Resources Observation And Science (EROS) Center (2017)
NBR	Normalized Burn Ratio	(NIR - SWIR2) / (NIR + SWIR2)	x	x	García and Caselles (1991)

NDRE1	Normalized Difference Red-edge Index 1	(RedEdge2 - RedEdge1) / (RedEdge2 + RedEdge1)		x	Gitelson and Merzlyak (1994)
NDRE2	Normalized Difference Red-edge Index 2	(RedEdge3 - RedEdge1) / (RedEdge3 + RedEdge1)		x	Ju *et al.* (2010)
NDRE3	Normalized Difference Red-edge Index 3	(RedEdge4 - RedEdge3) / (RedEdge4 + RedEdge3)		x	Navarro *et al.* (2017)
NDRS	Normalized distance red & SWIR	(DRS - DRSmin) / (DRSmax - DRSmin)	x	x	Huo *et al.* (2021); Earth Resources Observation And Science (EROS) Center (2017)
NDVI	Normalized Difference Vegetation Index	(NIR - Red)/(NIR + Red)	x	x	Rouse *et al*. (1974)
NDWI	Normalized Difference Water Index	(Green - NIR) / (Green + NIR)	x	x	McFEETERS (1996)
RDI	Simple Ratio MIR/NIR Ratio Drought Index	SWIR2 / NIR		x	Pinder and McLeod (1999)

Classified land cover data for 2010, 2015, and 2020 was gathered from the Spatialized Canadian National Forest Inventory (SCANFI) (Guindon *et al.* 2024). SCANFI is a collection of 30-meter resolution maps of forest attributes for Canada, including land cover type, forest canopy height, crown closure, aboveground tree biomass, deciduous tree cover, and fractional cover for several common tree species such as black spruce, jack pine, and lodgepole pine. SCANFI was developed using photo-interpreted high-resolution imagery, Landsat spectral imagery, and hundreds of regional land cover models (Guindon *et al.* 2024). Descriptions of the SCANFI predictor variables used in the analysis can be found in Table 2.

3.1.3.2 LiDAR-derived vegetation metrics

We calculated LiDAR-derived vegetation metrics from airborne LAS/LAZ point cloud data in NE Alberta, using the lidR package in R. As more Lidar becomes available we will do this for all of Alberta as well Point clouds were first normalized to height above ground using a k-nearest neighbour inverse-distance weighting algorithm. We then filtered the normalized point cloud classified vegetation points. Vegetation metrics were then computed at 5-m resolution using pixel-based aggregation. Standard height metrics (e.g., mean, maximum, and height percentiles) were generated, and we additionally computed custom vegetation metrics describing the vertical distribution of returns (Table 5). Metric rasters generated for each tile (defined as the spatial footprint of individual LAS/LAZ files) were mosaicked to form continuous LiDAR-derived vegetation surfaces.

Table 5: LiDAR vegetation derivatives included in the analyses. Metrics describe height distributions and the proportion of LiDAR returns within defined height bins.

Metric Name	Description
zmean	Mean vegetation height (m)
zsd	Standard deviation of vegetation height (m)
zmin	Minimum vegetation height (m)
zmax	Maximum vegetation height (m)
zq50	50th percentile vegetation height (m)
zq95	95th percentile vegetation height (m)
zq99	99th percentile vegetation height (m)
pzabovez3	Proportion of vegetation returns > 3 m (%)
pzabovez5	Proportion of vegetation returns > 5 m (%)
pzabovez10	Proportion of vegetation returns > 10 m (%)

pzabovez20	Proportion of vegetation returns > 20 m (%)
pz_1_to_3	Proportion of vegetation returns between 1 and 3 m (%)
pz_3_to_5	Proportion of vegetation returns between 3 and 5 m (%)
pz_5_to_10	Proportion of vegetation returns between 5 and 10 m (%)
pz_10_to_20	Proportion of vegetation returns between 10 and 20 m (%)

For all predictor variables, we calculated the mean and standard deviation within 100-, 500-, and 1000-m buffers around each point count location.

3.1.4 Analyses

PIWO occupancy models were generated using BRTs following the methods of Elith *et al.* (2008) and the dismo and gbm packages in R (Greenwell *et al.* 2022, Hijmans *et al.* 2023). BRTs were chosen over alternative modeling methods, such as general linear mixed models, due to their superior predictive performance, effective handling of non-linearity and high-order interactions, and lack of a priori assumptions (Craig and Huettmann 2009, McCue *et al.* 2014). QPAD detectability offsets were included in the BRTs to control for survey-level differences in Pileated Woodpecker detectability (Solymos *et al.* 2013). The dataset was randomized to eliminate patterns that could bias model training.

To account for spatial and temporal structure in the data, each survey location was assigned to a spatio-temporal block. Spatial blocks were created using a hexagonal grid with 150-km spacing, and temporal blocks were defined using quantile-based year bins. These were combined into unique spatio-temporal blocks, which were used to stratify both the train/test data and the assignment of bootstrap IDs, ensuring that each resample included a representative set of sites from across all spatial and temporal blocks.

Models were generated using the following multi-step process: (1) Optimal hyperparameters were identified through a grid search combined with 10-fold cross-validation (Table 6). A total of 108 models were evaluated, covering all possible combinations of hyperparameter values. The final hyperparameters were selected based on the model with the lowest RMSE. (2) A BRT model was then trained using the tuned hyperparameters with the gbm.step function from the dismo package in R. (3) The dismo::gbm.simplify function was used to iteratively remove low-contributing predictor variables, minimizing predictive deviance. (4) The model hyperparameters were retuned using the reduced set of predictor variables. (5) The final model was trained using the gbm.step function with tuned hyperparameters and refined set of predictors. We generated 100 bootstrap iterations of a final model. (6) Performance of the acoustic model for predicting where PIWO would be heard was assessed using both 10-fold cross-validation and a 75/25 training–test split for each of the 100 model bootstraps. Validation focused on metrics commonly used for presence–absence species distribution models — the true skill statistic (TSS), Cohen's kappa, and area under the curve (of the ROC) (AUC) — and prediction error was quantified using root mean square error (RMSE), mean square error (MSE), and log loss. (7) Spatial prediction rasters were generated using the dismo::predict function and a prediction grid created by calculating mean focal statistics for each predictor variable using a 500-meter circular moving window. Spatial predictions were generated for each bootstrap model, and summary prediction rasters were calculated from the mean and standard deviation of bootstrap model predictions.

Table 6: Hyperparameter values tested for the BRT models (Greenwell *et al.* 2022).

Hyperparameter	**Settings**	**Definition**
shrinkage	[0.001, 0.01, 0.1]	The learning rate.
interaction.depth	[2, 3]	The maximum depth of each tree (i.e. the level of variable interactions).
n.minobsinnode	[10, 15, 20, 30, 50, 100]	Minimum number of observations required in a terminal node.
bag.fraction	[0.5, 0.75, 0.85]	The fraction of data used to fit each tree.

This multistep modelling pipeline was applied across a suite of predictor variable sets representing different combinations of land cover, bioclimatic, vegetation structure, Landsat bands and indices, Sentinel-2 bands and indices, and their various pairwise and combined integrations. In total, twenty distinct predictor sets were evaluated, ranging from land-cover–only models to full models incorporating all Landsat, Sentinel-2, and land-cover predictors.

We conducted a second validation of the predictive models using field-mapped locations of cavity-bearing trees based on where you might hear a PIWO. In other words, we assessed if the sound map could be used to find cavities. We compared predicted suitability at known cavity locations (n = 706) to suitability at 4,000 randomly sampled background points. Model performance was evaluated using 100 bootstrap iterations, where each iteration resampled 4,000 background points and extracted predicted probabilities for both cavity and background locations. For each iteration, we assessed model performance using discrimination metrics (AUC, Kolmogorov–Smirnov statistic, Wilcoxon rank-sum test), probability-error metrics (Brier score, log-loss), and the mean predicted probabilities for cavity versus background points. We then summarized the mean and standard deviation of each metric across bootstraps to evaluate how consistently the model assigns higher suitability to cavity locations than to background sites.

In addition to the Alberta-level models, we developed LiDAR-based sub-models to refine predictions. For each predictor set, point-level occupancy probabilities from the final BRT model were combined with LiDAR metrics and used as inputs to the sub-models. These sub-models followed the same multi-step modelling pipeline but relied solely on main-model predictions and LiDAR metrics to predict habitat suitability.

3.2 Results

Here, we present results from four of the twenty models evaluated, representing increasing combinations of remote-sensing predictors: a land cover–only model, a Landsat-only model, a combined Landsat + land cover model, and an integrated Landsat + land cover + Sentinel-2 model. The land cover model provided a baseline level of performance, with a mean cross-validated deviance of 1.226 ± 0.004, explaining 7.29% ± 0.32% of the deviance, and achieving a mean AUC of 0.811 ± 0.006. The Landsat model, which incorporated spectral indicators of vegetation productivity and canopy stress, performed similarly, with a deviance of 1.231 ± 0.005, deviance explained of 6.89% ± 0.37%, and an AUC of 0.808 ± 0.006, indicating that Landsat spectral information alone can provide similar performance to land cover based models. Integrating Landsat indices with land cover produced slightly stronger performance, with a deviance of 1.228 ± 0.004, deviance explained of 7.12% ± 0.29%, and an AUC of 0.814 ± 0.006, although gains were modest. The highest-performing model was the fully integrated Landsat + land cover + Sentinel-2 model, which achieved a mean deviance of 1.220 ± 0.004, explained 7.71% ± 0.30% of the deviance, and reached an AUC of 0.820 ± 0.006. Although the strongest model of the four, improvements over the Landsat + land cover model were small. Taken together, these results indicate that while both Landsat and Sentinel-2 data contribute to model performance, improvements are limited.

In addition to out-of-sample cross-validation, we evaluated the top-performing model by comparing the locations of cavity-bearing trees found during 2024–2025 field surveys and random background locations. Cavities were observed more often in regions the model suggested were more favourable for Pileated Woodpecker drumming, and model validation showed strong discrimination between cavity locations of all sizes and randomly sampled background points (AUC = 0.83). Model performance varied by cavity size class, with strong discrimination for small to mid-sized cavities (AUC = 0.85–0.87) and moderate discrimination for larger cavities more likely to be excavated by Pileated Woodpeckers (>7.6 cm; AUC = 0.78–0.79) (Table 7). Together, these results suggest that the acoustic-based occupancy model captures broad habitat conditions associated with cavity occurrence across a range of cavity sizes. The strong correspondence between predicted suitability and field observations confirms that the key habitat features emphasized by the model—mature mixedwood and aspen forests with tall, heterogeneous canopies—are effective for prioritizing cavity search areas. However, cavities occur across a wide range of predicted suitability values (Figure 3). Therefore, while the map (Figure 4) is useful for guiding field searches, survey effort should target a range of habitat conditions rather than only the highest-ranked areas.

Table 7. Performance metrics (AUC, Brier score, log loss) for the top-performing acoustic-based habitat model evaluated using cavity-bearing tree locations from 2024–2025 field surveys, summarized by cavity size class.

Cavity Size Class	AUC	Brier Score	Log Loss
All cavities	0.836	0.143	0.919
2.5 to 5 cm cavities	0.868	0.131	0.921
5 to 7.6 cm cavities	0.849	0.132	0.984
7.6 to 10.2 cm cavities	0.778	0.133	0.989
> 10.2 cm cavities	0.786	0.129	0.989

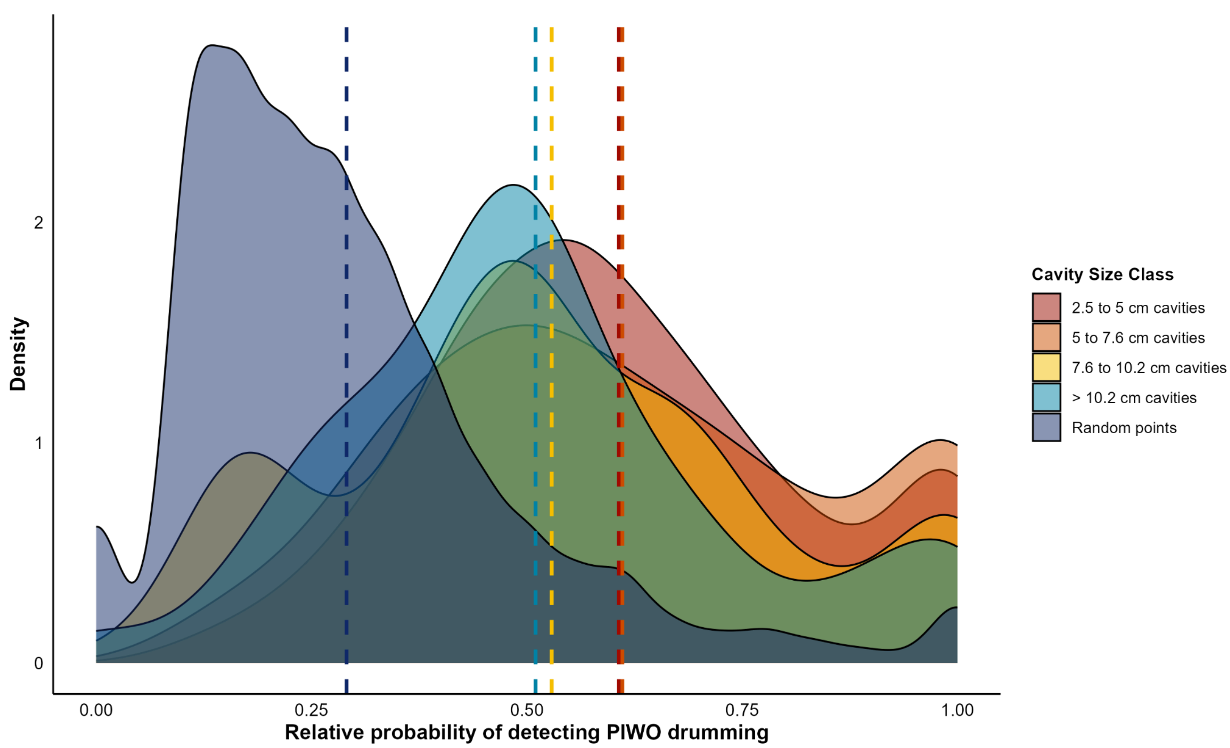

Figure 3. Density distributions of predicted habitat suitability for cavity-bearing tree locations (by cavity size class) and randomly sampled background points.

It is unclear why the model performed less well for larger cavities, and more data are needed to understand these results. Possible explanations include (1) temporal mismatch between when cavities were excavated and the forest conditions captured by contemporary remote-sensing data, as large cavities can persist for many years, and (2) detection biases in field surveys that favour large cavities in more accessible or visually open areas.

We attempted to build LiDAR-based sub-models to refine habitat predictions by combining point-level habitat suitability predictions from the above models with high-resolution LiDAR. However, LiDAR variables were consistently dropped during the model simplification process, indicating that they provided little additional predictive value. As a result, the LiDAR sub-models showed no improvement in predictive performance over the broader scale models. This supports that, in Alberta, the primary drivers of Pileated Woodpecker habitat selection are the presence of older aspen and mixedwood stands, which are already well captured by the land cover and spectral predictors used in the main models.

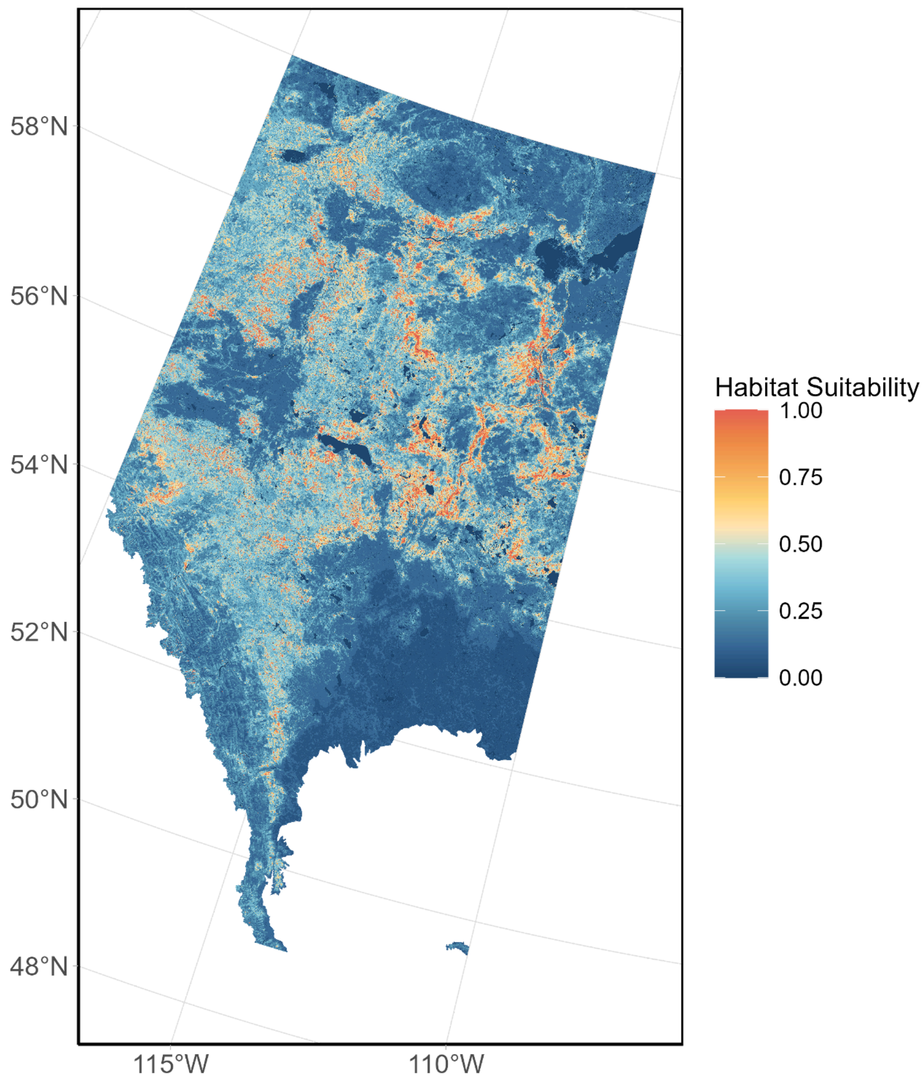

Figure 4: Predicted habitat suitability for Pileated Woodpecker across Alberta based on the integrated Landsat + land cover + Sentinel-2 model. Warmer colours indicate a higher probability of detecting woodpecker drumming and a greater likelihood of suitable habitat.

3.3 Informing Fieldwork

In 2024, we began using the predictive map (Figure 4) and random stratified sampling to select search locations representing high, medium, and low PIWO occupancy levels. During the summer of 2024 and 2025, these areas were systematically searched for PIWO cavity trees, using search protocols developed by Simran Bains. To support ground-based searches for nest cavities, we classified the 30-m occupancy-probability raster from the top-performing habitat model into four fixed suitability bins (0–0.25, 0.25–0.5, 0.5–0.75, 0.75–1.0), representing low, medium, high, and very high predicted occupancy. Within the area, we then drew a stratified random sample of raster cells by independently selecting points from each suitability class. Each selected point was converted into a 1-ha sampling unit by centering a 100 × 100 m square on its coordinates, consistent with the field search protocol.

4. Search Protocol

A detailed protocol for searching for PIWO cavities can be found in Appendix A. In areas of interest, surveyors search a standardized area of 1 hectare by dividing each hectare block into transects with a pair of individuals walking about 10-15 metres apart searching every tree for a cavity. Our protocol for transect searches has been used by various groups, such as the Cities of Edmonton and Red Deer, Government of Alberta, and consulting companies (LGL LTD. And Vertex). Locations of all cavities and foraging trees are collected in order to provide an estimate of cavity density which helps understand the commonality of PIWO cavities which is key to understanding how limiting they may or may not be. Each hectare search takes a minimum of 30 minutes but can be longer depending on the amount of deadline and density of shrubs. An app was created that can be used by anyone to track cavities. This app also includes the ability to track randomly located cavities. Please contact us for more information if you require more information. Available at: [https://five.epicollect.net/project/albertapiwosearchtool.](https://five.epicollect.net/project/albertapiwosearchtool)

5. Cavity Surveys

5.1 Methods

Using the PIWO acoustic occupancy map ver. 0.10), we selected areas to conduct 1 ha block surveys in 2024 and 2025. Figure 5 shows the areas searched and all the cavities found between 2023-2025 across the province. Preselected areas were referred to as “systematic searches.” Random searches were those done opportunistically if surveyors were in an area with ideal habitat. In addition to 1 ha block searches, we also recorded incidental cavities as we found them during the field seasons when walking between study sites (detailed protocol can be found in the Appendix A).

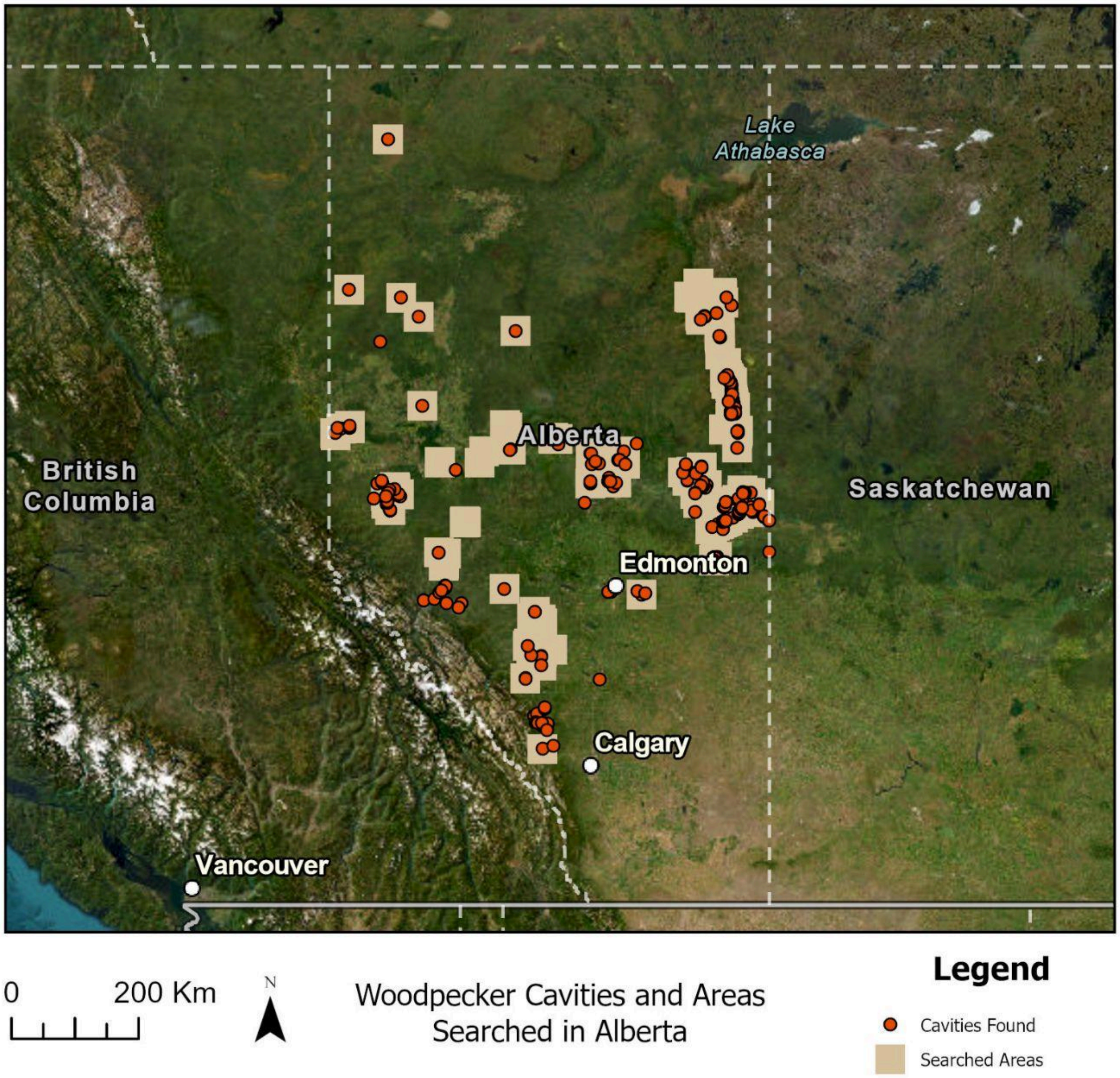

Figure 5. Map of all woodpecker cavities and areas searched from 2023-2025 across the province.

5.1.1 How to Identify Viable vs Non-viable Cavities

Viable cavities are those that can be used for nesting because they are deep enough (~25–60 cm); on the other hand, non-viable cavities are not suitable for nesting because they are not deep enough. We identified viable cavities by using a wireless cavity inspection camera on a 50 ft. telescopic pole and examining whether there was a bowl present or not (i.e. the cavities were deep or not). Due to the size of the camera, only cavities with entrance diameters of ~7 cm or greater could be inspected. If cavities were viable, the camera was able to give a clear image of what was inside, whereas if they were not viable, the camera would not be able to focus and capture a clear image.

5.2 Results

An estimated 1,180 hectares were searched between 2024-2025 in Alberta. Figure 6 shows the distribution of cavities per hectare. The mean number of cavities found per ha was 0.5 (SD 1.34). The overall cavity densities by cavity size classes are summarized in Table 8. PIWO sized cavities are less abundant than small cavities. Cavities in the 7.6-10.2 cm and > 10.2 classes had densities of 0.049 cavities/ha and 0.019 cavities/ha, respectively. These results suggest larger cavities are less common than smaller cavities.

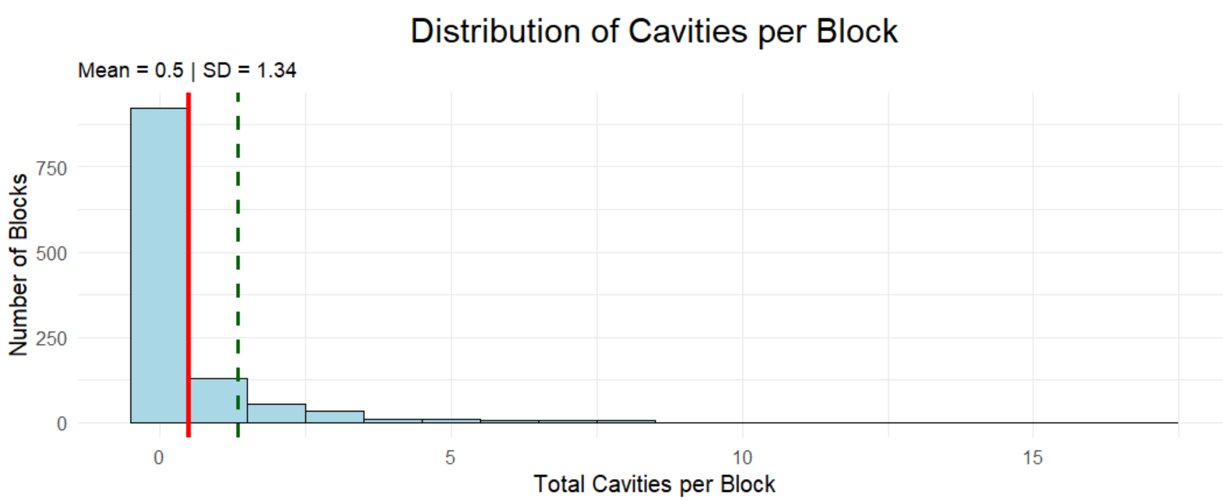

Figure 6: Distribution of cavities found per hectare block. The red line represents the mean, while the green represents the standard deviation.

Table 8: Density of cavities by size.

Cavity Diameter (cm)	Count	Density per ha
2.5 - 5.0	258	0.139
5.0 - 7.6	205	0.110
7.6 - 10.2	92	0.049
Over 10.2	36	0.019

5.2.1 Cavities found based on PIWO Acoustic Occupancy Model

Cavities found in different PIWO occupancy levels are shown in Table 9. We used a Poisson generalized linear model to test whether the number of cavities differed based on occupancy, with each hectare treated as a replicate. Results for the models are summarized in Table 10.

Table 9: Number of cavities found in each PIWO occupancy level by cavity diameter.

Occupancy Level	2.5-5.0 cm	5.0-7.6 cm	7.6-10.2 cm	> 10.2 cm
0 to 0.25	11	9	4	2
0.25 to 0.50	87	67	29	21
0.50 to 0.75	98	64	36	6
0.75 to 1.0	61	64	23	7

Table 10: Poisson Model results based on cavity size.

Poisson Model	AIC
Total cavities	3131.881
2.5 to 5 cm cavities	1673.748
5 to 7.6 cm cavities	1422.311
7.6 to 10.2 cm cavities	791.209
> 10.2 cm cavities	381.006

5.2.2 PIWO Sized Cavities

In this report, cavities greater than 7.6 cm are treated as cavities potentially excavated by PIWO. 77% of these cavities were found in Trembling Aspen. Table 11 summarizes the mean tree height and DBH for these cavities, while Table 12 shows the proportion of cavities based on tree decay classification used by Blanc and Martin (2012). Large cavities were found in all classes of decay — the highest proportion were found in class 6, which accounted for 22% of cavity trees. Additionally, 29% of cavities were found in live or unhealthy trees (classes 1 and 2). When grouped together and compared with other classes (3-8), logistic regression indicates that large cavities are more likely to be found in live or unhealthy trees than dead or decaying trees ($p = 0.0012$).

Table 11: Mean tree height and DBH measurements for large cavities.

Cavity Diameter (cm)	Mean Tree Height (m)	Mean DBH (cm)
7.6 - 10.2	28.7	44.30
Over 10.2	20.6	44.6

Table 12: Proportion of large cavities based on tree decay classification.

Tree Decay Class	Number of Cavities	Proportion of cavities
1 - Live and healthy with little biotic/abiotic damage	23	0.180

2 - Live and unhealthy (e.g. broken top, shelf fungus, boring insects, trunk gall)	15	0.117
3 - Recently dead (most branches/twigs, possible broken top, stable)	19	0.148
4 - No needles/twigs (50% branches lost, possible broken top, 25-50% bark lost, wood mostly hard)	8	0.063
5 - Most branches gone (possible broken top, 51-75% bark lost, wood hard and soft)	14	0.109
6 - No branches (some stubs, broken top, 76-100% bark lost, wood mostly soft)	28	0.219
7 - No branches (broken top, no bark, wood soft)	14	0.109
8 - No branches (broken top, no bark, hollow/partially hollow shell)	7	0.055

5.3 Discussion

Based on our findings, the largest cavities were rare to find compared to smaller cavities. More specifically, the density of PIWO sized cavities were low, with 7.6 - 10.2 cm cavities occurring at a density of 0.049 cavities/ha, and cavities greater than 10.2 at 0.019 cavities/ha. This suggests that PIWO cavities are limited across the landscape. In addition, many cavities nearing PIWO size can be found in areas with occupancy levels greater than 0.5. While PIWO is typically associated with mature forest stands, they can also be found in younger forests and developed areas if large trees are present (Cooke and Hannon 2012). Residual forest patches retained during harvesting often include cavity trees and feeding snags as they are left during harvest events. Therefore, occupancy levels less than 0.5 should be considered in surveys for PIWO cavities even though PIWO themselves may no longer be there based on the sound model. Furthermore, decay-class analysis showed that large cavities were more likely to be found in live or unhealthy trees than indead and decaying ones. While this is consistent with previous work on PIWO cavity availability and nest-site selection (Bonar 2001, Cooke and Hannon 2012), tree condition and identity of likely secondary users needs to be better understood. For this, we started to revisit cavities this past summer (2025) and will continue this for the next 2 years. We plan to revisit cavities within each decay class and monitor their reuse rate in order to provide a model that can be used to decide what is the likelihood that a located cavity is likely to be used within a three-year period.

5.3.1 Challenges and limitations

We found many cavities in areas not covered by the PIWO acoustic occupancy map ver. 0.10. Cavity density is highest in the habitat that the PIWO acoustic signal deems the best. However, that habitat is relatively uncommon across the landscape. As a result, the absolute number of cavities in the landscape will be cumulatively higher in medium and low occupancy level habitats because these habitats are more abundant. This finding stresses the need for more validation of large cavities in lower quality PIWO habitat to ensure they are truly PIWO cavities. This will require far more revisits with a peeper camera and evaluation of how often the cavities are actually used by PIWO or other species. As well, our models need additional work to identify other attributes of cavity trees and snags that exist in low to medium quality PIWO habitat (i.e. look for features of snags in cutblocks), potentially by using more refined LiDAR data (but see section 6).

While developing methods for cavity surveys, we found that many people including professional consultants had a difficult time identifying cavities in the field and the species that excavated those cavities. To address the challenge of species identification, we asked surveyors to estimate the diameter of each cavity they found. The reasoning for this is the larger cavities are more likely to have been excavated by PIWO but could have been excavated by other species.

Additionally, there are some logistical and resource constraints when conducting cavity surveys. Grid surveys can be very time consuming, especially in areas with many potential cavity trees. While this survey method may not be the most effective way of finding cavities, it was important to see how much effort is needed to find cavities. Meandering searches can find cavities, however then we would have a limited understanding of cavity density which is important for understanding if they are a limiting resource. Further, the boreal region in Alberta has many Aspen/Poplar trees and cavities can be difficult to find. Therefore, a lot of time needs to be invested in cavity searches. In addition to time needed in the field, some teams either did not have a camera to look inside cavities; or they were limited to a look inside cavities of a certain height because their camera was attached to a wire. This makes it difficult for field crews to determine if a cavity is viable or not and this can be a key determinant of whether action to protect the observed cavity is actually needed.

5.3.2 Management Implications

To ensure compliance with the MBCA, we suggest that habitats with low or very low occupancy levels should not be ignored in surveys as they contain many PIWO sized cavities. Additionally, retaining large live and decaying trees where possible may help maintain trees that could potentially be excavated by PIWO and reused by protected species.

5.4 Data availability

Cavity and search area data is available through our Google Earth Engine application (see Section 10). Additionally, all raw data is stored on Epicollect and has been shared with CNRL members and Vertex (assisted in collecting data during surveys).

6. Cavity-Bearing Tree Model

To assess if we could find the individual trees that had PIWO cavities, we also developed a crown-level cavity-bearing tree suitability model to flag trees most likely to contain Pileated Woodpecker cavities. This analysis used the provincial Pileated Woodpecker occupancy model predictions described in Section 3, together with field-mapped cavity and nest locations, LiDAR tree crown metrics, and spectral indicators of tree health.

6.1 Methods

6.1.1 Cavity and nest tree data

Cavity and nest trees were mapped using high-accuracy Global Navigation Satellite System (GNSS). For each tree, observers recorded species, decay class, and approximate DBH. We treated crowns intersecting at least one cavity or nest as used (cavity = 1) and all other crowns within surveyed LiDAR tiles as available (cavity = 0).

6.1.2 Individual crown delineation and LiDAR metrics

LiDAR preprocessing followed the same general workflow described for LiDAR-derived vegetation metrics in Section 3.1.3.1 (height normalization, filtering to vegetation returns, and removal of high outliers, etc.), but was extended to delineate individual tree crowns using the lidR package in R. We generated a 0.5 m canopy height model (CHM) for each tile, smoothed the CHM with a 2.5 m moving window, and detected treetops using a 5 m local maximum filter. Individual trees were segmented from the normalized point cloud using the Dalponte algorithm, and crown boundaries were delineated by fitting concave hulls to the LiDAR points for each tree. For each crown, we calculated LiDAR metrics analogous to those summarized in Table 5 but at the crown rather than pixel scale. We summarized spectral indices and forest composition variables for each crown, including the Normalized Distance Red & SWIR index (NDRS) from Sentinel-2 as an indicator of canopy stress (Table 4).

6.1.3 Cavity suitability models and mapping

To evaluate whether crown-level LiDAR improved cavity prediction, we tested two modelling approaches:

(1) We paired each field-mapped cavity-bearing tree location (n=71) with the LiDAR-identified crown it intersected with and compared these “used” crowns to all other "available" crowns. This produced a use–availability dataset in which individual tree-level attributes (height, crown area, structural metrics, spectral indicators, and predicted aspen probability) were used to discriminate cavity trees from nearby non-cavity trees.

(2) We took a neighbourhood-level approach that summarized local crown structure and spectral characteristics around each cavity. For every cavity-bearing tree location, we calculated mean LiDAR-derived crown metrics within a 100 m radius (e.g., average crown height, variability in crown structure) and 500 m summaries of crown-level spectral indicators of canopy stress and productivity (e.g., NDVI, NDRS and red-edge indices). We then compared these neighbourhood summaries to equivalent metrics calculated around randomly selected background points. This approach was designed to test whether cavity occurrence is better explained by broader neighbourhood conditions—such as clusters of tall aspen with spectral signs of decay.

For both approaches, we fit boosted regression tree models using the multi-step workflow described in Section 3.1.4, adapting the predictor set to match the scale of each analysis. In the tree-level (use–availability) models, predictors included crown-level LiDAR structural metrics, spectral indicators, and predicted aspen probability for each delineated crown. In the neighbourhood-level models, predictors consisted of the 100-m summaries of LiDAR-derived crown structure and spectral characteristics surrounding each cavity or background point. In both cases, models were trained and tuned using the same hyperparameter search, cross-validation, and bootstrap procedures used in the Alberta-wide habitat models.

6.2 Results

To evaluate whether LiDAR data could improve our ability to identify cavity-bearing trees or refine cavity-suitability predictions, we tested two modelling approaches: a tree-level analysis linking cavities to individual crowns, and a neighbourhood-level analysis summarizing crown attributes around each cavity.

Preliminary results from both approaches indicate limited added predictive value from LiDAR-derived crown metrics.

The first (tree-level) modelling approach failed to converge. This could be due to the small number of cavity-bearing trees used in the analysis and temporal or spatial misalignment between cavity locations and the LiDAR crown data. For example, cavities may be found in older snags where the current LiDAR and spectral characteristics no longer reflect the tree conditions present when the cavity was originally selected.

For the second (neighbourhood-level) approach, the cavity suitability models showed no meaningful improvement in predictive performance compared to the provincial acoustic-based habitat models. Most of the LIDAR predictors were dropped during model simplification due to their low contribution to model performance, and the most influential predictors continued to be those forest composition and structural predictors that were already used in the provincial model (e.g., older aspen and mixedwood stands with tall, heterogeneous canopies). These results mirror those from the LiDAR sub-models described in Section 3.2 and suggest that LiDAR metrics do not provide additional predictive power beyond the original acoustic-based habitat model.

A limitation of the neighbourhood-level approach was the close proximity of some cavity-bearing trees, which led to overlap among some of the 100-m buffers. This overlap may have reduced the contrast between cavity and background neighbourhoods, weakening the model's ability to discriminate between them.

However, the tree crown layers could be useful for fieldwork, providing a map of the largest trees (especially large aspen and early-decay individuals most likely to be cavity-bearing) within a suitable area and can help crews target suitable trees during on-the-ground field surveys (Figure 7). These crown-level models will be updated as additional cavity data are collected in future field seasons. Our current conclusion until more data becomes available is that detailed individual tree models cannot determine which of two similar trees will have a PIWO cavity because similar trees tend to be found in the same area, especially in high suitability sites. However, in areas where there is a cavity tree this clumping of higher suitability trees could reduce search time as it helps more precisely locate areas where there is a greater number of potential trees that could hold cavities. In addition, having precise coordinates for these potential trees allows crews to focus their efforts more efficiently within each search area, rather than surveying the entire plot uniformly.

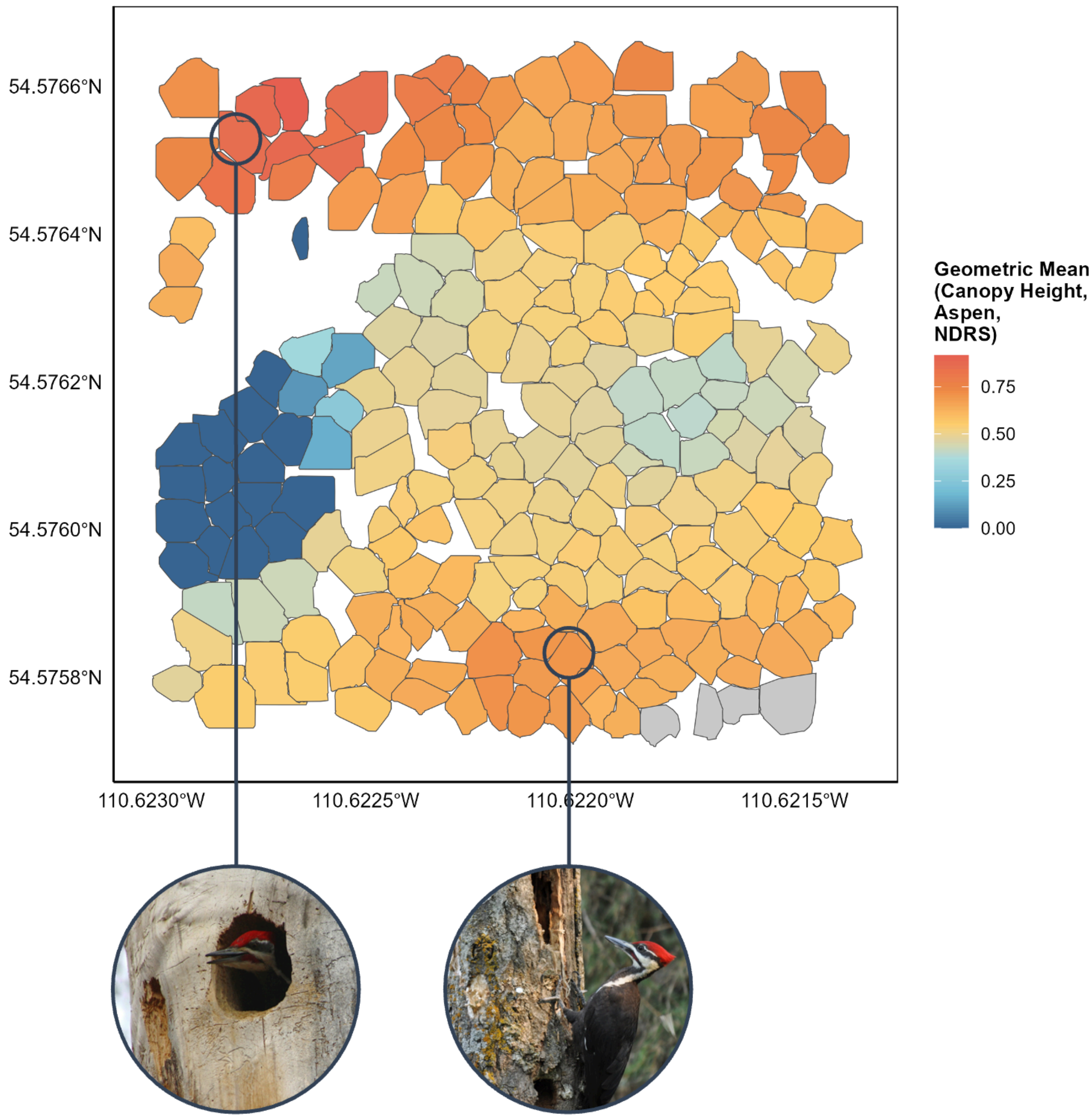

Figure 7: Individual tree crowns along a section of the proposed pipeline corridor, delineated from LiDAR and coloured by the geometric mean of three crown-level attributes: crown height, Sentinel-2 NDRS (a canopy-stress index), and the predicted probability of aspen.Warmer colours identify tall aspen crowns with spectral signs of stress (a combination of traits associated with Pileated Woodpecker cavity-bearing trees. The two circled crowns are examples of trees crowns flagged as high-potential: (insets) active Pileated Woodpecker cavities. They illustrate how crown-level metrics can direct ground searches toward the individual trees most likely to hold cavities or show woodpecker use. Although crown-level LiDAR metrics did not improve cavity suitability models, these layers remains a useful field aid for prioritizing high potential trees during surveys.

7. Monitoring Cavities (Ongoing)

For the past 5 years, the Bayne Lab and the Royal Alberta Museum have collaborated to monitor nest cavities for PIWO and Northern Flicker (NOFL). The inclusion of NOFL is important in monitoring because PIWO may excavate these cavities more to reuse (Martin *et al.* 2004). The purpose of monitoring cavities long-term is to better understand cavity reuse and longevity.

In 2025 we were able to revisit 40 cavities around the province. The interior of each cavity was inspected with a wireless camera. Out of these 40 cavities, we were able to confirm 10 that were being reused. We plan to continue to revisit more cavities for the next 3 years (minimum) so that we can collect enough data to model which cavities are viable and reused. More data is required before we can model the factors that predict reuse by other species.

8. Evaluating Drumming Behavior

8.1 Methods

In 2022 we developed methods for using autonomous recording units (ARU) to locate drumming and vocalizing PIWO. We determined that visual scanning ARU data using Wildtrax was the most cost-effective data processing method to assess if PIWO are using an area (compared to listening and the automated recognizer BirdNET). We are now comparing visual scanning to a new bird ID system we created called Hawk Ears. Near the optimal time of the year and day (April 2 and 1 hour from sunrise), processing ~40 – 1 minute recordings ensures that you have 95% certainty that the species is or is NOT using that location. To get to 99% certainty it takes about ~60 recordings. In summer 2022, we placed ARUs in the following configuration: 1) at a known and active PIWO nest; 2) at known PIWO feeding sites; 3) and at random locations. At the PIWO nests we placed ARU 50 m, 100 m, and 400 m away to see how detection radius influences the number of PIWO calls or drums that are detected. In 2023, we deployed ARUs around 14 feeding snags and 33 woodpecker cavities.

We processed the ARU data evaluating how many drums, sounds made by striking their bills on hard surfaces, and vocalizations of PIWO are observed at different times of the year at active PIWO nests, old PIWO nests, foraging trees, other woodpecker nests, and random locations. The goal was to determine whether the number of acoustic signals, the ratio of drumming versus vocalization, the occurrence of juvenile sounds, and the timing of the various acoustic signals can be used to predict the approximate location of nests of PIWO. We are currently processing these same sites for the entire community using the automated recognizer HawkEars. The rationale is that an ARU could be put in place before any type of land management is required to determine if a PIWO OR any migratory bird capable of using a cavity is present. If a sufficiently robust model can be created then the need for nest searching will be reduced. Recent studies on Common Nighthawks show that the different sounds they produce can inform where to look for nests (Knight et al. 2022).

Woodpeckers show similar behaviors and have more vocalizations that can be used to determine where nests are more likely. More data is required to ensure this model is robust.

8.2 Results

Chi-square results show that there is a statistically significant difference between the vocalization types detected at nests, feeding, and random sites (X-squared = 2067.1, df = 6, $p < 2.2e-16$). Next, we examined how well we can predict cavity type using multinomial regression models. The best fit model used drums, adult calls, juvenile calls and distance to the cavity as predictor variables (AIC 36.9). Additionally, the combination of drums and adult calls gives additional information beyond each behavior on its own. Below is a table summarizing the models that were tested. Each predictor was tested individually before combining them to create interactions. Out of all single predictors, the models indicate that calls help predict cavity type.

Table 13: multinomial regression models tested.

Formula	Residual deviance	AIC
Cavity type ~ Non-vocal	154.85	162.85
Cavity type ~ Juvenile Call	159.47	167.47
Cavity type ~ Adult Call	55.27	63.27
Cavity type ~ Distance from cavity	32.11	36.11
Cavity type ~ Non-vocal + Juvenile Call + Adult Call	46.17	62.17
Cavity type ~ Non-vocal + Juvenile Call + Adult Call + Distance from cavity	27.77	37.77
Cavity type ~ Non-vocal * Adult Call + Juvenile Call + Distance from cavity	24.9	36.9
Cavity type ~ Non-vocal * Juvenile Call + Adult Call + Distance from cavity	27.51	39.51
Cavity type ~ Adult Call * Juvenile Call + Non-vocal + Distance from cavity	27.77	37.77
Cavity type ~ Non-vocal * Juvenile Call * Adult Call + Distance from cavity	20.39	40.39

8.3 Next steps

Our plan is to use acoustic cues of secondary cavity users to improve our model. Additionally, our goal is to build a model that can estimate the distance an ARU is from a cavity using a probability-based model. In order to do this, we deployed over 100 ARUs in 2025 at various distances from recently active cavities. These ARUs will also continue recording in April 2026.

9. Camera Deployment Experiment

9.1 Background

Camera traps are widely used in ecology to monitor wildlife, estimate population size, and analyze activity patterns. However, camera effectiveness depends on factors including animal body size and distance from the camera. Previous research has shown that cameras tend to record fewer images of smaller animals and animals that are farther away (DeWitt & Cocksedge 2023). While camera traps have been effective in studying terrestrial mammals, their limitations in detecting avian species remain underexplored. Studies have not investigated how well cameras capture bird activity from a distance, especially in tree canopies. Aguiar-Silva et al. demonstrated that remote cameras can be effective for monitoring Harpia harpyja (harpy eagle; 2017). Furthermore, accessing canopy nests and activity heights is expensive, requiring extensive technical training, equipment, and time. Due to bird migration patterns and seasonal behaviors, data collection is often limited to a few months meaning, annual data collection needs to be time efficient (Murgui, 2007). Ground-based camera deployments could reduce time, expenses, and dangers associated with tree climbing. While remote cameras are beneficial for avian ecology, their potential and limits for gathering data must be tested. Few studies have systematically evaluated the ability for motion-activated cameras to detect birds at varying heights and distances. Comparative research has typically focused on the ability of cameras to detect mammals or has involved birds at close range.

To address this gap, we are currently examining how different camera placements, with varying heights, and distances from the feeder, also mounted with a camera, affect detection rates. Ultimately, this study aims to improve camera trapping methods for monitoring canopy species and allow for avian research to be more accessible.

9.2 Methods

The objective of this study was to evaluate the detection performance of Reconyx Hyperfire cameras in capturing images of birds at varying distances and heights. The study is being conducted using a field setup involving bird feeders and multiple wildlife cameras mounted on trees and posts in rural, urban, and suburban areas in Alberta, Canada. Each plot consisted of four camera stations positioned around a suet feeder baited with woodpecker seedcake (Figure 8). The middle of the suet cage was fixed at a distance of 25 cm from the feeder camera lens, serving as a control. The other cameras are Infra-red cameras deploying a minimum of 5 m away from the feeder to replicate field deployments compared to the number of photos at this feeder camera. There are currently cameras deployed for this experiment, while data collected from retrieved sites are currently on WildTrax being processed. We plan to select more sites for our experiment in the next 2 years.

Figure 8: Setup of camera field experiment. Cameras (C) at mig-height and ground level were attached to trees or posts using a wooden platform with a camera mount (A), and secured with a python lock (B). For this experiment, we are pointing the cameras at feeders (D) to mimic birds coming to a cavity. At the feeder, there is an additional camera (E) pointing at the feeder to capture "true" detections up close.

10. Google Earth Engine Web Application

Our results are sharable via a Google Earth Engine web application (Figure 9). The platform provides a single access point for PIWO habitat maps, cavity data, and current modelling and fieldwork progress.

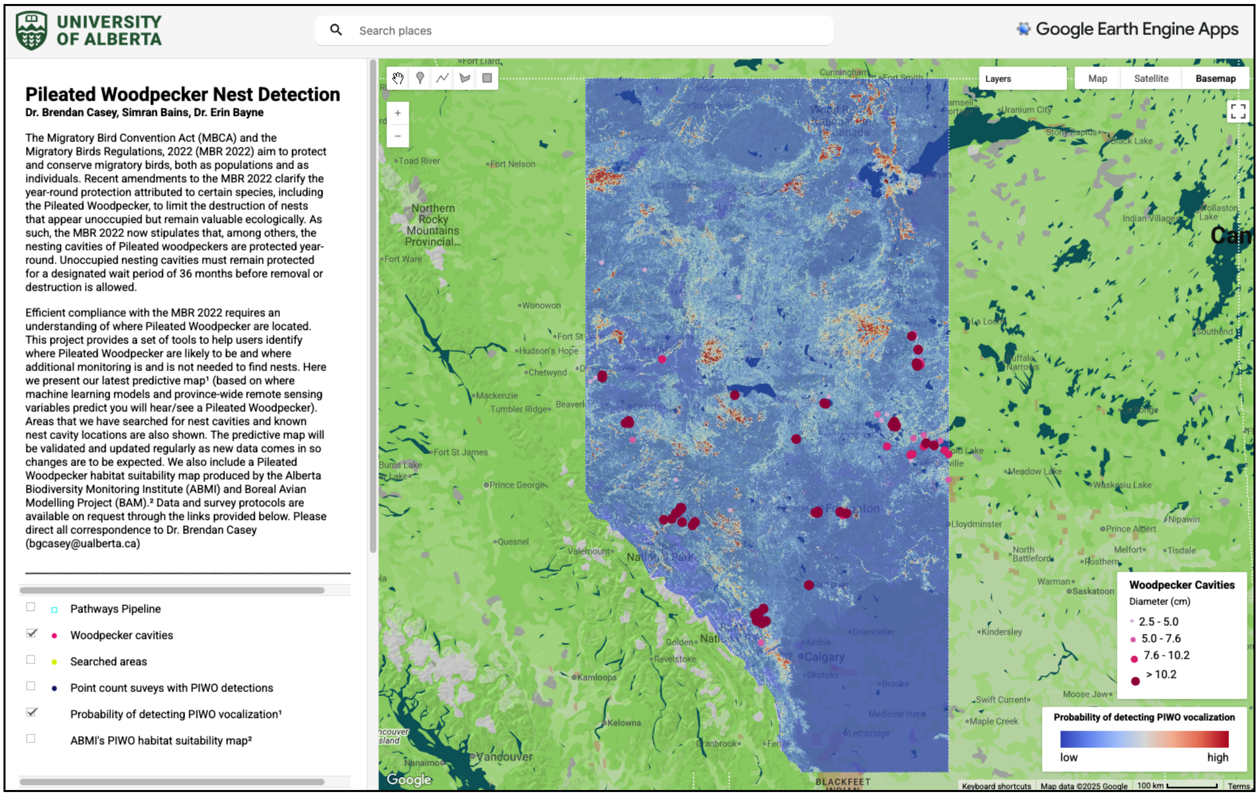

Figure 9: Image of the Google Earth Engine web application displaying the predicted habitat suitability for Pileated Woodpecker across Alberta and known cavity-bearing tree locations. Click here to visit.

11. Future Plans

We will continue to validate the predictive map using acoustic data from ARUs deployed across the province. Processing available acoustic data is currently underway. Regarding the acoustic model, our goal is to include vocalizations of secondary cavity users. Additionally, we aim to build a model that can estimate the distance an ARU is from a cavity using a probability-based model. In order to do this, we deployed over 100 ARUs in 2025 at various distances from recently active cavities. These ARUs will also continue recording in April 2026. Regarding cavity reuse, we will plan to revisit as many cavities as possible in the next 3 years to model reuse by cavity nesters.

We will continue to support the development of LiDAR-based cavity-bearing tree models by integrating new field data as it becomes available.

12. References

Blance, L.A and Martin, K. 2012. Identifying suitable woodpecker nest trees using decay selection profiles in trembling aspen (*Populus tremuloides*). Forest Ecology and Management 286:192-202.

Bonar, R.L. 2000. Availability of Pileated Woodpecker Cavities and Use by Other Species. Journal of Wildlife Management. 64:52 – 59.

Bonar, R.L. 2001. Pileated Woodpecker Habitat Ecology in Alberta Foothills [PhD Dissertation]. University of Alberta.

Bull, E.L. and J.A. Jackson. 2020. Pileated Woodpecker (*Dryocopus pileatus*), version 1.0. In Birds of the World (A. F. Poole, Editor). Cornell Lab of Ornithology, Ithaca, NY, USA.

Craig, E., and F. Huettmann. 2009. Using "blackbox" algorithms such AS TreeNET and random forests for data-ming and for finding meaningful patterns, relationships and outliers in complex ecological data: An overview, an example using g. Pages 65–84 *in* H.-F. Wang, editor. Intelligent data analysis. IGI Global.

Cooke, H. and S.J. Hannon. 2012. Nest-site selection by old boreal forest cavity excavators as a basis for structural retention guidelines in spatially-aggregated harvests. Forest Ecology and Management. 8:37-51.

Drapeau, P., A. Nappi, L. Imbeau, and M. Saint-Germain. Standing deadwood for keystone bird species in the eastern boreal forest: managing for snag dynamics. The Forestry Chronicles. 8(2):227-234.

Drever MC, Aitken KEH, Norris AR, and Martin K. 2008. Woodpeckers as reliable indicators of bird richness, forest health and harvest. Biological Conservation. 141:624-634.

Earth Resources Observation And Science (EROS) Center. 2017. Sentinel. U.S. Geological Survey.

Elith, J., J. R. Leathwick, and T. Hastie. 2008. A working guide to boosted regression trees. Journal of animal ecology 77:802–813.

García, M. J. L., and V. Caselles. 1991. Mapping burns and natural reforestation using thematic mapper data. Geocarto International 6:31–37.

Gitelson, A. A., Y. Gritz †, and M. N. Merzlyak. 2003. Relationships between leaf chlorophyll content and spectral reflectance and algorithms for non-destructive chlorophyll assessment in higher plant leaves. Journal of Plant Physiology 160:271–282.

Gitelson, A. A., Y. J. Kaufman, and M. N. Merzlyak. 1996. Use of a green channel in remote sensing of global vegetation from EOS-MODIS. Remote Sensing of Environment 58:289–298.

Gitelson, A., and M. N. Merzlyak. 1994. Spectral reflectance changes associated with autumn senescence of aesculus hippocastanum l. And acer platanoides l. Leaves. Spectral features and relation to chlorophyll estimation. Journal of Plant Physiology 143:286–292.

Government of Canada. 2023. Fact sheet: Nest Protection under the Migratory Birds Regulations, 2022. [Access December 12, 2023].

Guindon, L., F. Manka, D. L. P. Correia, P. Villemaire, B. Smiley, P. Bernier, S. Gauthier, A. Beaudoin, J. Boucher, and Y. Boulanger. 2024. A new approach for spatializing the Canadian national forest inventory (SCANFI) using landsat dense time series. Canadian Journal of Forest Research:cjfr-2023-0118.

Hoyt S. F. 1957. The Ecology of the Pileated Woodpecker. Ecology. 38(2):246 – 256.

Huete, A. 1997. A comparison of vegetation indices over a global set of TM images for EOS-MODIS. Remote Sensing of Environment 59:440–451.

Huo, L., H. J. Persson, and E. Lindberg. 2021. Early detection of forest stress from european spruce bark beetle attack, and a new vegetation index: Normalized distance red & SWIR (NDRS). Remote Sensing of Environment 255:112240.

Ju, C.-H., Y.-C. Tian, X. Yao, W.-X. Cao, Y. Zhu, and D. Hannaway. 2010. Estimating leaf chlorophyll content using red edge parameters. Pedosphere 20:633–644.

Ke A., Cedeño E., Karubian J., Carrasco L., Castillo F., Gonzales F., and Karp D. S. 2023. Cavity-nesting birds are limited by nesting habitat in Neotropical agricultural landscapes. Biotropica 55:1045 – 1057.

Knight E.C., R.M. Brigham, and E.M. Bayne. 2022. The Big Boom Theory: The Common Nighthawk wing-boom display delineates exclusive nesting territories. Ornithology. 139:1 – 10.

Lang, N., W. Jetz, K. Schindler, and J. D. Wegner. 2022. A high-resolution canopy height model of the earth. arXiv preprint arXiv:2204.08322.

Maltman, J. C., T. Hermosilla, M. A. Wulder, N. C. Coops, and J. C. White. 2023. Estimating and mapping forest age across Canada's forested ecosystems. Remote Sensing of Environment 290:113529.

Martin K. and J. M. Eadie. 1999. Nest webs: A community-wide approach to the management and conservation of cavity-nesting forest birds. Forest Ecology and Management. 115:243 – 257.

Matin K., K.E.H. Aitken, and K.L. Wiebe. 2004. Nest sites and nest webs for cavity-nesting communities in interior British Columbia, Canada: Nest characteristics and niche partitioning. Condor 106:5 – 109.

McCue, A. J., M. J. McGrath, and Y. F. Wiersma. 2014. Benefits and drawbacks of two modelling approaches for a generalist carnivore: Can models predict where Wile E. Coyote will turn up next? International Journal of Geographical Information Science 28:1590–1609.

McFEETERS, S. K. 1996. The use of the normalized difference water index (NDWI) in the delineation of open water features. International Journal of Remote Sensing 17:1425–1432.

Natural Regions Committee. 2006. Natural regions and subregions of Alberta. Compiled by DJ Downing; WW Pettapiece. Government of Alberta, Edmonton, Alberta, Canada.

Navarro, G., I. Caballero, G. Silva, P.-C. Parra, Á. Vázquez, and R. Caldeira. 2017. Evaluation of forest fire on madeira island using sentinel-2A MSI imagery. International Journal of Applied Earth Observation and Geoinformation 58:97–106.

Pinder, J. E., and K. W. McLeod. 1999. Indications of relative drought stress in longleaf pine from thematic mapper data. Photogrammetric Engineering & Remote Sensing 65:495–501.

Province of Alberta. 2000a. Public lands act.

Province of Alberta. 2000b. Wildlife act.Rouse, J. W., R. H. Haas, J. A. Schell, and D. W. Deering. 1974. Monitoring vegetation systems in the great plains with ERTS. NASA Spec. Publ 351:309.

Sørensen, R., and J. Seibert. 2007. Effects of DEM resolution on the calculation of topographical indices: TWI and its components. Journal of Hydrology 347:79–89.

Yamazaki, D., D. Ikeshima, J. Sosa, P. D. Bates, G. H. Allen, and T. M. Pavelsky. 2019. MERIT hydro: A high-resolution global hydrography map based on latest topography dataset. Water Resources Research 55:5053–5073.

Appendix A

Survey Site Selection

Cavity surveys were conducted at selected points across Alberta. In some cases, field teams also conducted opportunistic searches at random sites where large aspen trees or signs of woodpecker activity were observed.

Survey Design

Some survey locations were paired with ARUs, while others were searched independently. Teams conducted a standardized cavity search within a 1-hectare plot (100 m × 100 m). Each plot was divided into transects and surveyors walked up and down each transect as they looked around every tree for cavities (Figure 10). When possible, transects were oriented north–south to avoid looking into the sun and to improve visibility of cavity entrances.

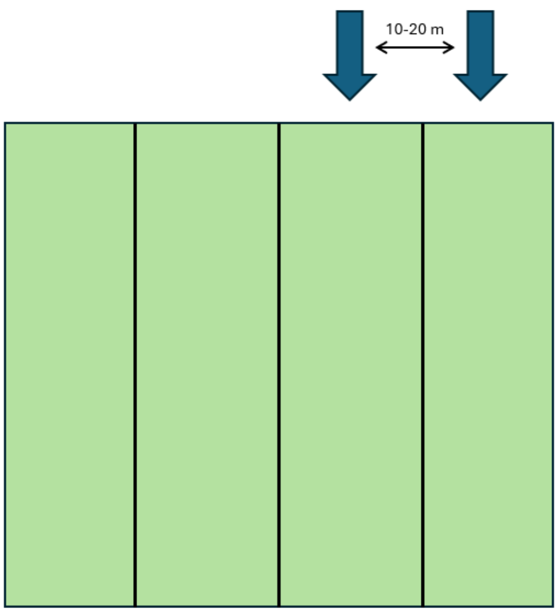

Figure 10: Diagram of hectare block survey.

To ensure complete coverage of each hectare, surveyors spaced themselves parallel to each other (10-20 m apart) and remained within visual contact (spacing distance varied with vegetation density). This approach ensured consistent inspection of all trees and reduced the likelihood of missing cavities.

Field Data Collection

Field teams used Epicollect forms to document observations. Within each hectare, teams photographed the site from two random locations, taking pictures in the four cardinal directions. Surveyors also recorded:

- Feeding signs
- Presence and estimated diameter of cavity entrance holes
- Tree species in which cavities were located
- Notes on incidental cavity discoveries outside of systematic searches

The Epicollect form contained three survey types:

- **Systematic** – full-hectare searches conducted around preselected points
- **Random** – hectare-scale searches conducted in areas with suitable large trees
- **Incidental** – opportunistic cavity detections outside search plots

Once a cavity was located, surveyors used a cavity inspection camera ("tree peeper") to photograph the interior of cavities ~ 7 cm or greater in diameter. This is because the camera cannot fit into smaller entrances. Cavities were classified as viable or non-viable based on the presence of a nesting bowl or other structural features.

Tree and Cavity Measurements

For each cavity tree, the following measurements and attributes were recorded:

- GPS location
- Tree species
- Tree height
- Diameter at breast height (DBH)
- Live crown ratio (length of live crown / total height)
- Canopy cover
- Cavity height above ground
- Orientation of entrance hole(s)
- Condition of each entrance hole (e.g., fresh excavation, wood chips at base)
- Decay class based on Blanc & Martin (2012), using the following categories:
    1. Live, healthy
    2. Live but unhealthy (broken top, fungi, insect damage, trunk gall)
    3. Recently dead, most branches retained
    4. Dead with 50% branch loss, 25–50% bark loss, wood mostly hard
    5. Dead with 51–75% bark loss; wood both hard and soft
    6. Dead, no branches, 76–100% bark loss, wood mostly soft
    7. Dead, no bark, broken top, wood soft
    8. Dead, hollow or partially hollow shell